

## Polarized Blazar X-rays imply particle acceleration in shocks

Ioannis Liodakis<sup>1\*</sup>, Alan P. Marscher<sup>2</sup>, Iván Agudo<sup>3</sup>, Andrei V. Berdyugin<sup>4</sup>, Maria I. Bernardos<sup>3</sup>, Giacomo Bonnoli<sup>3,5</sup>, George A. Borman<sup>6</sup>, Carolina Casadio<sup>7,8</sup>, Víctor Casanova<sup>3</sup>, Elisabetta Cavazzuti<sup>9</sup>, Nicole R. Caverio<sup>10</sup>, Laura Di Gesu<sup>9</sup>, Niccoló Di Lalla<sup>11</sup>, Immacolata Donnarumma<sup>9</sup>, Steven R. Ehlert<sup>12</sup>, Manel Errando<sup>10</sup>, Juan Escudero<sup>3</sup>, Maya García-Comas<sup>3</sup>, Beatriz Agís-González<sup>3</sup>, César Husillos<sup>3</sup>, Jenni Jormanainen<sup>1,4</sup>, Svetlana G. Jorstad<sup>2,13</sup>, Masato Kagitani<sup>14</sup>, Evgenia N. Kopatskaya<sup>15</sup>, Vadim Kravtsov<sup>4</sup>, Henric Krawczynski<sup>10</sup>, Elina Lindfors<sup>1</sup>, Elena G. Larionova<sup>15</sup>, Grzegorz M. Madejski<sup>16</sup>, Frédéric Marin<sup>17</sup>, Alessandro Marchini<sup>18</sup>, Herman L. Marshall<sup>53</sup>, Daria A. Morozova<sup>15</sup>, Francesco Massaro<sup>19,20</sup>, Joseph R. Masiero<sup>21</sup>, Dimitri Mawet<sup>22</sup>, Riccardo Middei<sup>23,24</sup>, Maxwell A. Millar-Blanchaer<sup>25</sup>, Ioannis Myserlis<sup>26</sup>, Michela Negro<sup>27,28</sup>, Kari Nilsson<sup>1</sup>, Stephen L. O'Dell<sup>12</sup>, Nicola Omodei<sup>11</sup>, Luigi Pacciani<sup>29</sup>, Alessandro Paggi<sup>19,20,30</sup>, Georgia V. Panopoulou<sup>31</sup>, Abel L. Peirson<sup>11</sup>, Matteo Perri<sup>23,24</sup>, Pierre-Olivier Petrucci<sup>32</sup>, Juri Poutanen<sup>4,33</sup>, Simonetta Puccetti<sup>9</sup>, Roger W. Romani<sup>11</sup>, Takeshi Sakanai<sup>14</sup>, Sergey S. Savchenko<sup>15,34,35</sup>, Alfredo Sota<sup>3</sup>, Fabrizio Tavecchio<sup>5</sup>, Samaporn Tinyanont<sup>36</sup>, Andrey A. Vasiliev<sup>15</sup>, Zachary R. Weaver<sup>2</sup>, Alexey V. Zhovtan<sup>6</sup>, Lucio A. Antonelli<sup>24,23</sup>, Matteo Bachetti<sup>37</sup>, Luca Baldini<sup>38,39</sup>, Wayne H. Baumgartner<sup>12</sup>, Ronaldo Bellazzini<sup>38</sup>, Stefano Bianchi<sup>40</sup>, Stephen D. Bongiorno<sup>12</sup>, Raffaella Bonino<sup>19,20</sup>, Alessandro Brez<sup>38</sup>, Niccoló Bucciantini<sup>41,42,43</sup>, Fiamma Capitanio<sup>29</sup>, Simone

Castellano<sup>38</sup>, Stefano Ciprini<sup>23,44</sup>, Enrico Costa<sup>29</sup>, Alessandra De Rosa<sup>29</sup>, Ettore Del Monte<sup>29</sup>, Alessandro Di Marco<sup>29</sup>, Victor Doroshenko<sup>33,45</sup>, Michal Dovčiak<sup>46</sup>, Teruaki Enoto<sup>47</sup>, Yuri Evangelista<sup>29</sup>, Sergio Fabiani<sup>29</sup>, Riccardo Ferrazzoli<sup>29</sup>, Javier A. Garcia<sup>48</sup>, Shuichi Gunji<sup>49</sup>, Kiyoshi Hayashida<sup>50</sup>, Jeremy Heyl<sup>51</sup>, Wataru Iwakiri<sup>52</sup>, Vladimir Karas<sup>46</sup>, Takao Kitaguchi<sup>47</sup>, Jeffery J. Kolodziejczak<sup>12</sup>, Fabio La Monaca<sup>29</sup>, Luca Latronico<sup>19</sup>, Simone Maldera<sup>19</sup>, Alberto Manfreda<sup>38</sup>, Andrea Marinucci<sup>9</sup>, Giorgio Matt<sup>40</sup>, Ikuyuki Mitsuishi<sup>54</sup>, Tsunefumi Mizuno<sup>55</sup>, Fabio Muleri<sup>29</sup>, Stephen C.-Y. Ng<sup>56</sup>, Chiara Oppedisano<sup>19</sup>, Alessandro Papatto<sup>24</sup>, George G. Pavlov<sup>57</sup>, Melissa Pesce-Rollins<sup>38</sup>, Maura Pilia<sup>37</sup>, Andrea Possenti<sup>37</sup>, Brian D. Ramsey<sup>12</sup>, John Rankin<sup>29</sup>, Ajay Ratheesh<sup>29</sup>, Carmelo Sgró<sup>38</sup>, Patrick Slane<sup>58</sup>, Paolo Soffitta<sup>29</sup>, Gloria Spandre<sup>38</sup>, Toru Tamagawa<sup>47</sup>, Roberto Taverna<sup>59</sup>, Yuzuru Tawara<sup>54</sup>, Allyn F. Tennant<sup>12</sup>, Nicolas E. Thomas<sup>12</sup>, Francesco Tombesi<sup>60</sup>, Alessio Trois<sup>37</sup>, Sergey Tsygankov<sup>4,33</sup>, Roberto Turolla<sup>59,61</sup>, Jacco Vink<sup>62</sup>, Martin C. Weisskopf<sup>12</sup>, Kinwah Wu<sup>61</sup>, Fei Xie<sup>63,29</sup> and Silvia Zane<sup>61</sup>

\* [yannis.liodakis@utu.fi](mailto:yannis.liodakis@utu.fi).

<sup>1</sup>Finnish Centre for Astronomy with ESO, FI-20014 University of Turku, Finland.

<sup>2</sup>Institute for Astrophysical Research, Boston University, 725 Commonwealth Avenue, Boston, MA 02215, USA.

<sup>3</sup>Instituto de Astrofísica de Andalucía, IAA-CSIC, Glorieta de la Astronomía s/n, 18008 Granada, Spain.

<sup>4</sup>Department of Physics and Astronomy, FI-20014 University of Turku, Finland.

<sup>5</sup>INAF Osservatorio Astronomico di Brera, Via E. Bianchi 46, 23807 Merate (LC), Italy.

<sup>6</sup>Crimean Astrophysical Observatory RAS, P/O Nauchny, 298409, Crimea.

<sup>7</sup>Institute of Astrophysics, Foundation for Research and Technology - Hellas, Voutes, 7110 Heraklion, Greece.

<sup>8</sup>Department of Physics, University of Crete, 70013, Heraklion, Greece.

- <sup>9</sup>Agenzia Spaziale Italiana, Via del Politecnico snc, 00133 Roma, Italy.
- <sup>10</sup>Physics Department and McDonnell Center for the Space Sciences, Washington University in St. Louis, St. Louis, MO 63130, USA.
- <sup>11</sup>Department of Physics and Kavli Institute for Particle Astrophysics and Cosmology, Stanford University, Stanford, California 94305, USA.
- <sup>12</sup>NASA Marshall Space Flight Center, Huntsville, AL 35812, USA.
- <sup>13</sup>Laboratory of Observational Astrophysics, St. Petersburg University, University Embankment 7/9, St. Petersburg 199034, Russia.
- <sup>14</sup>Graduate School of Sciences, Tohoku University, Aoba-ku, 980-8578 Sendai, Japan.
- <sup>15</sup>Astronomical Institute, St.Petersburg State University, St. Petersburg, 198504, Russia.
- <sup>16</sup>Kavli Institute for Particle Astrophysics and Cosmology, Stanford University, and SLAC 2575 Sand Hill Road, Menlo Park, CA 94025, USA.
- <sup>17</sup>Université de Strasbourg, CNRS, Observatoire Astronomique de Strasbourg, UMR 7550, 67000 Strasbourg, France.
- <sup>18</sup>University of Siena, Department of Physical Sciences, Earth and Environment, Astronomical Observatory, Via Roma 56, 53100 Siena, Italy.
- <sup>19</sup>Istituto Nazionale di Fisica Nucleare, Sezione di Torino, Via Pietro Giuria 1, 10125 Torino, Italy.
- <sup>20</sup>Dipartimento di Fisica, Università degli Studi di Torino, Via Pietro Giuria 1, 10125 Torino, Italy.
- <sup>21</sup>Caltech/IPAC, 1200 E. California Blvd, MC 100-22, Pasadena, CA 91125, USA.
- <sup>22</sup>California Institute of Technology, MC 249-17, 1200 E. California Blvd., Pasadena, CA, 91125, USA.
- <sup>23</sup>Space Science Data Center, Agenzia Spaziale Italiana, Via del Politecnico snc, 00133 Roma, Italy.
- <sup>24</sup>INAF Osservatorio Astronomico di Roma, Via Frascati 33, 00040 Monte Porzio Catone (RM), Italy.
- <sup>25</sup>University of California, Santa Barbara, CA 93106, USA.
- <sup>26</sup>Institut de Radioastronomie Millimétrique, Avenida Divina Pastora, 7, Local 20, E-18012 Granada, Spain.

- <sup>27</sup>Center for Research and Exploration in Space Science and Technology (CRESST), Green-belt, MD 20771, USA.
- <sup>28</sup>Department of Physics and Center for Space Sciences and Technology, University of Maryland Baltimore County, Baltimore, MD 21250, USA.
- <sup>29</sup>INAF Istituto di Astrofisica e Planetologia Spaziali, Via del Fosso del Cavaliere 100, 00133 Roma, Italy.
- <sup>30</sup>INAF-Osservatorio Astrofisico di Torino, via Osservatorio 20, I-10025 Pino Torinese, Italy.
- <sup>31</sup>California Institute of Technology, MC 350-17, 1200 E. California Blvd., Pasadena, CA, 91125, USA.
- <sup>32</sup>Université Grenoble Alpes, CNRS, IPAG, 38000 Grenoble, France.
- <sup>33</sup>Space Research Institute of the Russian Academy of Sciences, Profsoyuznaya Str. 84/32, Moscow 117997, Russia.
- <sup>34</sup>Special Astrophysical Observatory, Russian Academy of Sciences, 369167, Nizhnii Arkhyz, Russia.
- <sup>35</sup>Pulkovo Observatory, St.Petersburg, 196140, Russia.
- <sup>36</sup>University of California Santa Cruz, 1156 High Street, Santa Cruz, CA 95064 USA.
- <sup>37</sup>INAF Osservatorio Astronomico di Cagliari, Via della Scienza 5, 09047 Selargius (CA), Italy.
- <sup>38</sup>Istituto Nazionale di Fisica Nucleare, Sezione di Pisa, Largo B. Pontecorvo 3, 56127 Pisa, Italy.
- <sup>39</sup>Dipartimento di Fisica, Università di Pisa, Largo B. Pontecorvo 3, 56127 Pisa, Italy.
- <sup>40</sup>Dipartimento di Matematica e Fisica, Università degli Studi Roma Tre, Via della Vasca Navale 84, 00146 Roma, Italy.
- <sup>41</sup>INAF Osservatorio Astrofisico di Arcetri, Largo Enrico Fermi 5, 50125 Firenze, Italy.
- <sup>42</sup>Dipartimento di Fisica e Astronomia, Università degli Studi di Firenze, Via Sansone 1, 50019 Sesto Fiorentino (FI), Italy.
- <sup>43</sup>Istituto Nazionale di Fisica Nucleare, Sezione di Firenze, Via Sansone 1, 50019 Sesto Fiorentino (FI), Italy.
- <sup>44</sup>Istituto Nazionale di Fisica Nucleare, Sezione di Roma Tor Vergata, Via della Ricerca Scientifica 1, 00133 Roma, Italy.
- <sup>45</sup>Institut für Astronomie und Astrophysik, Sand 1, 72076 Tübingen, Germany.
- <sup>46</sup>Astronomical Institute of the Czech Academy of Sciences, Boční II 1401/1, 14100 Praha 4, Czech Republic.

- <sup>47</sup>RIKEN Cluster for Pioneering Research, 2-1 Hirosawa, Wako, Saitama 351-0198, Japan.
- <sup>48</sup>California Institute of Technology, Pasadena, CA 91125, USA.
- <sup>49</sup>Yamagata University, 1-4-12 Kojirakawa-machi, Yamagata-shi 990-8560, Japan.
- <sup>50</sup>Osaka University, 1-1 Yamadaoka, Suita, Osaka 565-0871, Japan.
- <sup>51</sup>University of British Columbia, Vancouver, BC V6T 1Z4, Canada.
- <sup>52</sup>Department of Physics, Faculty of Science and Engineering, Chuo University, 1-13-27 Kasuga, Bunkyo-ku, Tokyo 112-8551, Japan.
- <sup>53</sup>MIT Kavli Institute for Astrophysics and Space Research, Massachusetts Institute of Technology, 77 Massachusetts Avenue, Cambridge, MA 02139, USA.
- <sup>54</sup>Graduate School of Science, Division of Particle and Astrophysical Science, Nagoya University, Furo-cho, Chikusa-ku, Nagoya, Aichi 464-8602, Japan.
- <sup>55</sup>Hiroshima Astrophysical Science Center, Hiroshima University, 1-3-1 Kagamiyama, Higashi-Hiroshima, Hiroshima 739-8526, Japan.
- <sup>56</sup>Department of Physics, University of Hong Kong, Pokfulam, Hong Kong.
- <sup>57</sup>Department of Astronomy and Astrophysics, Pennsylvania State University, University Park, PA 16801, USA.
- <sup>58</sup>Center for Astrophysics, Harvard & Smithsonian, 60 Garden St, Cambridge, MA 02138, USA.
- <sup>59</sup>Dipartimento di Fisica e Astronomia, Università degli Studi di Padova, Via Marzolo 8, 35131 Padova, Italy.
- <sup>60</sup>Dipartimento di Fisica, Università degli Studi di Roma Tor Vergata, Via della Ricerca Scientifica, 00133 Roma, Italy.
- <sup>61</sup>Mullard Space Science Laboratory, University College London, Holmbury St Mary, Dorking, Surrey RH5 6NT, UK.
- <sup>62</sup>Anton Pannekoek Institute for Astronomy & GRAPPA, University of Amsterdam, Science Park 904, 1098 XH Amsterdam, The Netherlands.
- <sup>63</sup>Guangxi Key Laboratory for Relativistic Astrophysics, School of Physical Science and Technology, Guangxi University, Nanning 530004, China.

Blazars are active galactic nuclei that launch collimated, powerful jets of magnetized relativistic plasma. Their primary jet, whose emission typically spans from low-frequency radio to very high-energy ( $\gtrsim 0.1$  TeV)  $\gamma$ -rays [1], is aligned towards our line of sight. Multiwavelength polarization is a crucial probe of the magnetic field structure and emission processes in such jets. Until now, sensitive polarization observations have been limited to the radio, infrared, and optical range, thereby leaving a gap in our knowledge of the physical conditions experienced by the most energetic particles. Here, we report the first-ever detection of X-ray polarization from the jet in an accreting supermassive black hole system, the blazar Markarian 501 (Mrk 501). The recently launched Imaging X-ray Polarimetry Explorer (*IXPE*, [2]) measures a linear polarization degree ( $\Pi$ ) over the 2–8 keV X-ray energy range of  $10 \pm 2\%$  with an electric vector position angle of  $134^\circ \pm 5^\circ$ , parallel to the radio jet. The X-ray  $\Pi$  is more than a factor of 2 higher than the optical  $\Pi$ . We conclude that an energy-stratified relativistic electron population, i.e., an acceleration scenario where the higher energy particles emit from more magnetically ordered regions closer to the acceleration site, is the most likely explanation of the higher degree of polarization at X-ray energies. A second *IXPE* observation conducted 16 days later yielded similar results, strengthening our conclusions.

It is well established that the low-energy emission in blazars is synchrotron radiation from relativistic particles. However, the mechanisms that energize the radiating particles are still elusive. This is in part due to the unknown ratio of anti-matter to matter in the jets [e.g., 3], as well as the diversity in emission behavior (e.g., correlated multiwavelength variability, [e.g., 4, 5]) among blazars. A particularly important diagnostic is the level of order of the magnetic field and its mean direction relative to the jet axis, which can be determined by measurements of the linear polarization. For example, the most common model used to explain the observed variable multiwavelength emission has been the shock-in-jet model [6], which predicts polarization vectors that are aligned with the jet, with  $\Pi$  decreasing with wavelength.

Much of the variability of blazar emission appears to be stochastic in nature, often modeled as a red noise process. Still, some of the observed patterns of polarization variability (e.g., electric vector position angle rotations) have been found to be inconsistent with purely stochastic processes [7, 8]. This indicates that there is some coherent ordering of the magnetic field, e.g., by compression or amplification by plasma processes in shocks [e.g., 9, 10] or by the presence of a global helical magnetic field component [e.g., 11–13]. On the other hand, multi-zone emission models, often involving a turbulent magnetic field, some of which include magnetic reconnection, can reproduce a number of the observed characteristics of the variable linear polarization at optical wavelengths [14–17, 24].

Multi-wavelength polarization data can advance our understanding of these processes, especially regarding the structure of the magnetic field in the jet's high-energy emission regions. Until now, polarization observations of extragalactic objects have been limited to radio, infrared, and optical wavelengths [e.g., 18–20]. X-ray polarimetry allows us to investigate the freshly accelerated particles and the magnetic fields they experience on much shorter time scales than radio and optical polarimetry. Given that electrons of Lorentz factor  $\gamma$  emit synchrotron radiation at frequencies  $\nu_s \propto \gamma^2$  but radiate their energy on the time scale of their synchrotron or Compton cooling time  $\tau_s \propto \gamma^{-1}$  implies that  $\tau_s \propto \nu_s^{-1/2}$ . X-ray polarization can thus track the evolution of the particle acceleration region(s) on  $\sim 3000$  and  $\sim 50$  times shorter time scales than in the radio band and optical band, respectively. These estimates assume a non-varying magnetic field, and that synchrotron cooling dominates over adiabatic cooling. For a decaying magnetic field, the difference in time scales will be broader. The recently launched *IXPE* offers a radically new way of studying the particle acceleration regions in relativistic outflows.

The first *IXPE* observation of Mrk 501 took place during 2022 March 8-10 (100 ksec, MJD 59646-59648) and was accompanied by observations across the electromagnetic spectrum from multiple observatories (see Methods). *IXPE* measured a polarization degree  $\Pi_X = 10 \pm 2\%$  and an electric vector position angle  $\psi_X = 134^\circ \pm 5^\circ$  (measured East of North) over the X-ray energy range of 2-8 keV. Contemporaneous radio-millimeter and optical observations (Table 3) measured  $\Pi_R = 1.5 \pm 0.5\%$  along  $\psi_R = 152^\circ \pm 10^\circ$  and  $\Pi_O = 4 \pm 1\%$  along  $\psi_O = 119^\circ \pm 9^\circ$ . A second *IXPE* observation took place 2022 March 26-28 (86 ksec, MJD 59664-59667) yielding  $\Pi_X = 11 \pm 2\%$  along  $\psi_X = 115^\circ \pm 4^\circ$ . Simultaneously to the second observation, the optical polarization was measured as  $\Pi_O = 5 \pm 1\%$  along  $\psi_O = 117^\circ \pm 3^\circ$  (Table 4). The two observed  $\psi_X$  are consistent within  $3\sigma$ . The radio and optical  $\psi$  also lie within  $3\sigma$  from each other and  $\psi_X$ . Moreover, the position angle of Mrk 501's jet has been determined through Very Long Baseline Array (VLBA) imaging at 43 GHz to be  $120^\circ \pm 12^\circ$  [21]. This would suggest that, in both cases, radio-to-X-ray  $\psi$  is aligned with the jet axis within uncertainties. We do not find evidence of polarization variability during either *IXPE* observation. Compared to the archival multiwavelength observations, we find the flux and polarization of Mrk 501, for both observations, to be within one standard deviation of the median of the long-term light curves. For the first *IXPE* observation the measured X-ray flux indicates an average activity state, while during the second observation we find evidence of an elevated X-ray flux state.

In Mrk 501, and similar blazars whose synchrotron spectral energy distribution peaks at X-ray frequencies, synchrotron radiation is the dominant emission process from radio to X-rays, although radiation at different wavelengths could possibly originate from different regions in the jet. This allows us to distinguish among several particle acceleration scenarios and their expected polarization patterns, and to compare them against our findings as summarized in Table 1. In the single-zone case - for example, the radiating particles

**Table 1** Summary of model properties. We find increasing  $\Pi$  towards higher frequencies, no significant variability during the 2-3 day long *IXPE* observations, and rough alignment of  $\psi$  with the jet axis from radio to X-rays. Therefore, a shock-accelerated, energy-stratified electron population model satisfies all our multiwavelength polarization observations.

Model	Multiwavelength polarization	X-ray polarization variability <sup>†</sup>	X-ray polarization angle
Single-zone	constant*	slow	any
Multi-zone	mildly chromatic	high	any
Energy stratified (shock)	strongly chromatic	slow	along the jet axis
Magnetic reconnection (kink instability)	constant	moderate	perpendicular to jet axis
Observed	strongly chromatic	slow	along the jet axis

\*There is a slight dependence on the slope of the emission spectrum.

<sup>†</sup>Slow variability = a few days to week, moderate variability = days, high variability  $\leq 1$  day.

are accelerated to highly relativistic energies confined within a plasmoid with a partially ordered or helical magnetic field. The global, perhaps helical, magnetic field structure is expected to produce similar polarization patterns across frequencies, with little variability over time [22]. If the field is helical,  $\psi$  should align with the jet direction for most viewing angles [11]. In an alternative scenario, particles become energized over a limited volume - e.g., at a shock front - and then advect or diffuse away from that region [6, 23, 24]. We refer to this model as “energy-stratified”. In this process, the electrons lose energy to radiation, and so emit at progressively decreasing frequencies. The magnetic field is expected to be more ordered over smaller volumes, in which case  $\Pi$  decreases toward lower frequencies (longer wavelengths), while  $\psi$  can vary with frequency if the mean direction of the magnetic field changes as the volume increases. In a turbulent region, roughly modeled as  $N$  cells, each with a uniform but randomly oriented field, we expect  $\Pi \sim 75\%/\sqrt{N}$ , with the value of  $\Pi$  exhibiting variability on short time-scales with a standard deviation  $\sim 0.5\Pi$  [14], as often observed [25]. Particles would be accelerated at a shock front that amplifies the magnetic field component that is parallel to the shock front. The decrease in  $\Pi$  and any change in  $\psi$  toward lower frequencies would provide information on whether the field beyond the shock relaxes to a direction parallel to the shock normal [10, 22] or becomes increasingly turbulent. For a turbulent field in the plasma crossing a shock front, particle acceleration would be most efficient in cells whose magnetic field is nearly parallel to the shock normal, leading to a higher value of  $\Pi$  and more pronounced variability at higher frequencies [14]. A third possibility is turbulence-induced particle acceleration within an emission zone in the jet, which can be caused by magnetic reconnection when contiguous regions of oppositely-directed magnetic field come into contact [26]. The passage of turbulent cells through the emission region would cause irregular variations, including some apparent rotations, in  $\psi$  [15, 27]. A fourth scenario, which may apply particularly to jets from blazars such as Mrk 501 with synchrotron peaks at X-ray frequencies, is magnetic reconnection where the jet

flow is sheared because of transverse velocity gradients [28]. Shearing would stretch the magnetic field along the jet boundary, so that  $\psi$  is expected to be transverse to the jet direction.

The polarization measurements reported here reveal an increase in  $\Pi$  toward higher frequencies, in tension with single-zone, turbulent multi-zone, and magnetic reconnection models discussed above (Fig. 1). There is no significant variability within the duration of the individual *IXPE* observations, contrary to the predicted behaviour if turbulent cells moved in and out of the emission region on time-scales of  $\lesssim 2$  days. On the other hand, the low ( $< 10\%$ ) optical and X-ray polarization suggests partial ordering of the local magnetic field, possibly due to the presence of stationary turbulence. The wavelength dependence and lack of variability of  $\Pi$ , plus constancy of  $\psi$  and its alignment with the jet direction, supports the basic shock model of particle acceleration (see Table 1 [6, 22, 29]). In this model, the shock partially orders the magnetic field of the plasma crossing the shock, with the ordering perpendicular to the shock normal. This causes the net polarization electric vector to be aligned with the jet. As the plasma advects away from the shock, it encounters increasingly turbulent plasma that lowers  $\Pi$  toward lower frequencies. This leads to the observed relation  $\Pi_X \sim 2\text{--}2.5\Pi_O$ . Previous intensely-sampled measurements of the polarization of Mrk 501 have found variations in  $\Pi_O$  by  $\pm 5\%$  and in  $\psi_O$  by  $\sim 50^\circ$  from one night to the next [25]. These apparently discrepant results can be reconciled if the turbulence of the plasma flowing through shocks in the jet is only intermittently time-variable, as has been found previously in other blazars [30]. One would also expect deviations of the observed  $\psi$  from the jet axis as one moves further away from the shock front into more turbulent regions of the jet. At present, the large  $\psi$  uncertainties prevent us from confirming such behavior. Future observations of Mrk 501 or similar blazars will allow us to explore the jet's multiwavelength polarization profile. A prediction of the energy-stratified model is that the X-ray polarization position angle of blazars like Mrk 501, will exhibit rotations [31].

In conclusion, we have shown that adding X-ray polarization to the already available radio and optical polarization diagnostics uniquely probes the physical conditions in supermassive black-hole systems. Future *IXPE* observations combined with dedicated modeling will allow for an in-depth exploration of the  $\Pi_X$ ,  $\psi_X$  variability in astrophysical jets.

**Acknowledgments.** I.L. thanks the Kavli Institute for the Physics and Mathematics of the Universe for their hospitality while this paper was written. The authors thank A. Veledina for discussions that helped improve this work. I.L. was supported by the JSPS postdoctoral short-term fellowship program. The Imaging X ray Polarimetry Explorer (*IXPE*) is a joint US and Italian mission. The US contribution is supported by the National Aeronautics and Space Administration (NASA) and led and managed by its Marshall Space Flight Center (MSFC), with industry partner Ball Aerospace (contract NNM15AA18C). The Italian contribution is supported by the Italian Space

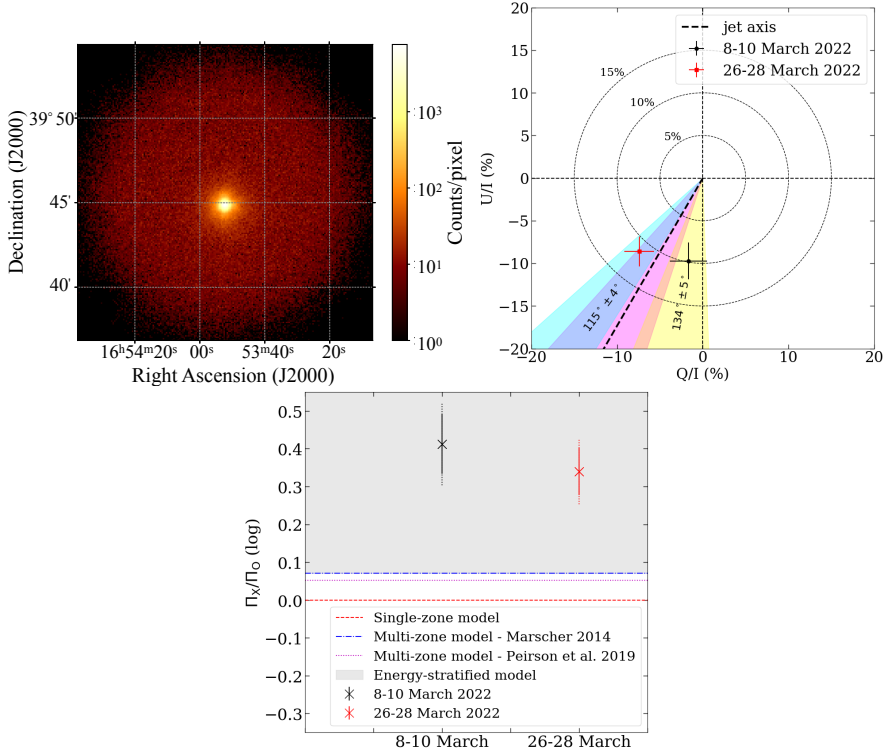


**Fig. 1** **Top left:** *IXPE* image of Mrk 501 during the 8-10 March 2022 observation in the 2-8 keV band. The colorbar denotes the number of X-ray photons per pixel. **Top right:** Normalized Stokes Q and Stokes U parameters of both *IXPE* observations. The yellow and cyan shaded regions denote the uncertainty (68% CI) in the polarization angle for the 8-10 March and 26-28 March observations respectively. The dashed black line shows the jet direction and the magenta shaded area its uncertainty (68% CI). The dashed circles mark different levels of polarization degree, as labeled. **Bottom:** Comparison between the observed logarithm of the X-ray and optical II ratio and the expectations from single-zone (red dashed line), two turbulent multi-zone jet models (dash-dotted blue and dotted magenta lines), and energy-stratified models (grey shaded area) for both *IXPE* observations (black for 8-10 March and red for 26-28 March). The solid errorbars show the ratio uncertainty from the *IXPE* measurements; the dotted errorbars show the full uncertainty including optical uncertainties.

Agency (Agenzia Spaziale Italiana, ASI) through contract ASI-OHBI-2017-12-I.0, agreements ASI-INAF-2017-12-H0 and ASI-INFN-2017.13-H0, and its Space Science Data Center (SSDC), and by the Istituto Nazionale di Astrofisica (INAF) and the Istituto Nazionale di Fisica Nucleare (INFN) in Italy. This research used data products provided by the IXPE Team (MSFC, SSCD, INAF, and INFN) and distributed with additional software tools by the High-Energy Astrophysics Science Archive Research Center (HEASARC), at NASA Goddard Space Flight Center (GSFC). Data from the Steward Observatory spectropolarimetric monitoring project were used. This program is supported by Fermi Guest Investigator grants NNX08AW56G, NNX09AU10G,

NNX12AO93G, and NNX15AU81G. This research has made use of data from the RoboPol programme, a collaboration between Caltech, the University of Crete, IA-FORTH, IUCAA, the MPIfR, and the Nicolaus Copernicus University, which was conducted at Skinakas Observatory in Crete, Greece. The IAA-CSIC co-authors acknowledge financial support from the Spanish "Ministerio de Ciencia e Innovacion (MCINN) through the "Center of Excellence Severo Ochoa" award for the Instituto de Astrofísica de Andalucía-CSIC (SEV-2017-0709). Acquisition and reduction of the POLAMI and MAPCAT data was supported in part by MICINN through grants AYA2016-80889-P and PID2019-107847RB-C44. The POLAMI observations were carried out at the IRAM 30m Telescope. IRAM is supported by INSU/CNRS (France), MPG (Germany) and IGN (Spain). The research at Boston University was supported in part by National Science Foundation grant AST-2108622, NASA Fermi Guest Investigator grant 80NSSC21K1917, and NASA Swift Guest Investigator grant 80NSSC22K0537. This study uses observations conducted with the 1.8 m Perkins Telescope Observatory (PTO) in Arizona (USA), which is owned and operated by Boston University. Based on observations obtained at the Hale Telescope, Palomar Observatory as part of a continuing collaboration between the California Institute of Technology, NASA/JPL, Yale University, and the National Astronomical Observatories of China. This research made use of Photutils, an Astropy package for detection and photometry of astronomical sources (Bradley et al., 2019). GVP acknowledges support by NASA through the NASA Hubble Fellowship grant #HST-HF2-51444.001-A awarded by the Space Telescope Science Institute, which is operated by the Association of Universities for Research in Astronomy, Incorporated, under NASA contract NAS5-26555. Based on observations made with the Nordic Optical Telescope, owned in collaboration by the University of Turku and Aarhus University, and operated jointly by Aarhus University, the University of Turku and the University of Oslo, representing Denmark, Finland and Norway, the University of Iceland and Stockholm University at the Observatorio del Roque de los Muchachos, La Palma, Spain, of the Instituto de Astrofísica de Canarias. The data presented here were obtained [in part] with ALFOSC, which is provided by the Instituto de Astrofísica de Andalucía (IAA) under a joint agreement with the University of Copenhagen and NOT. VK thanks Vilho, Yrjö and Kalle Väisälä Foundation. J.J. was supported by Academy of Finland project 320085. E. L. was supported by Academy of Finland projects 317636 and 320045. Part of the French contributions is supported by the Scientific Research National Center (CNRS) and the French spatial agency (CNES). Based on observations collected at the Observatorio de Sierra Nevada, owned and operated by the Instituto de Astrofísica de Andalucía (IAA-CSIC). Based on observations collected at the Centro Astronómico Hispano-Alemán(CAHA), proposal 22A-2.2-015, operated jointly by Junta de Andalucía and Consejo Superior de Investigaciones Científicas (IAA-CSIC).

**Corresponding author.** I. Liodakis, JSPS International Research Fellow, yannis.liodakis@utu.fi,

**Author contributions.** I. Liodakis coordinated the multiwavelength observations, performed the analysis and led the writing of the paper. H. Krawczynski, A. P. Marscher, L. Peirson, P. Petrucci, J. Poutanen, F. Tavecchio, and R. Romani contributed with discussion and parts of the paper. I. Agudo, C. Casadio, J. Escudero, and I. Myserlis contributed with the radio-millimeter polarization data. B. Agís-González, I. Agudo, A. V. Berdyugin, M. Bernardos, G. Bonnoli, V. Casanova, M. G. Comas, C. Husillos, J. Jormanainen, V. Kravtsov, E. Lindfors, I. Liodakis, K. Nilsson, S. S. Savchenko, and A. Sota contributed with the optical polarization data. G. V. Panopoulou contributed the infrared polarization data. A. P. Marscher, G. M. Madejski, R. Middei, L. Pacciani, M. Perri, and S. Puccetti contributed the *Swift* and *NuSTAR* data. L. Di Gesu, N. di Lalla, I. Donnarumma, S. R. Ehlert, H. L. Marshall, R. Middei, M. Negro, N. Omodei, A. Paggi, and A. L. Peirson, contributed with the *IXPE* analysis. The remaining authors are part of the multiwavelength follow-up and *IXPE* teams whose significant contribution made the multiwavelength polarization observations possible.

**Competing interests.** Authors declare that they have no competing interests.

**Data availability.** The data that support the findings of this study are available from the corresponding author upon request.

## References

- [1] Blandford, R., Meier, D. & Readhead, A. Relativistic Jets from Active Galactic Nuclei. *ARA&A* **57**, 467–509 (2019). <https://doi.org/10.1146/annurev-astro-081817-051948>, <https://arxiv.org/abs/1812.06025> [astro-ph.HE].
- [2] Weisskopf, M. C. *et al.* Imaging X-ray Polarimetry Explorer: prelaunch. *Journal of Astronomical Telescopes, Instruments, and Systems* **8** (2), 1 – 28 (2022). URL <https://doi.org/10.1117/1.JATIS.8.2.026002>. <https://doi.org/10.1117/1.JATIS.8.2.026002> .
- [3] Liodakis, I., Blinov, D., Potter, S. B. & Rieger, F. M. Constraints on magnetic field and particle content in blazar jets through optical circular polarization. *MNRAS* **509** (1), L21–L25 (2022). <https://doi.org/10.1093/mnras/slab118>, <https://arxiv.org/abs/2110.11434> [astro-ph.HE].
- [4] Liodakis, I. *et al.* Multiwavelength cross-correlations and flaring activity in bright blazars. *MNRAS* **480** (4), 5517–5528 (2018). <https://doi.org/10.1093/mnras/sty2264>, <https://arxiv.org/abs/1808.05625> [astro-ph.HE].
- [5] Liodakis, I., Romani, R. W., Filippenko, A. V., Kocevski, D. & Zheng, W. Probing Blazar Emission Processes with Optical/Gamma-Ray Flare Correlations. *ApJ* **880** (1), 32 (2019). <https://doi.org/10.3847/1538-4357/>

- ab26b7, <https://arxiv.org/abs/1905.11418> [astro-ph.HE].
- [6] Marscher, A. P. & Gear, W. K. Models for high-frequency radio outbursts in extragalactic sources, with application to the early 1983 millimeter-to-infrared flare of 3C 273. *ApJ* **298**, 114–127 (1985). <https://doi.org/10.1086/163592> .
- [7] Kiehlmann, S., Blinov, D., Pearson, T. J. & Lioudakis, I. Optical EVPA rotations in blazars: testing a stochastic variability model with RoboPol data. *MNRAS* **472**, 3589–3604 (2017). <https://doi.org/10.1093/mnras/stx2167>, <https://arxiv.org/abs/1708.06777> [astro-ph.HE].
- [8] Blinov, D. *et al.* RoboPol: connection between optical polarization plane rotations and gamma-ray flares in blazars. *MNRAS* **474**, 1296–1306 (2018). <https://doi.org/10.1093/mnras/stx2786>, <https://arxiv.org/abs/1710.08922> [astro-ph.HE].
- [9] Hughes, P. A., Aller, H. D. & Aller, M. F. Polarized radio outbursts in BL Lacertae. II. The flux and polarization of a piston-driven shock. *ApJ* **298**, 301–315 (1985). <https://doi.org/10.1086/163611> .
- [10] Tavecchio, F., Landoni, M., Sironi, L. & Coppi, P. Probing shock acceleration in BL Lac jets through X-ray polarimetry: the time-dependent view. *MNRAS* **498** (1), 599–608 (2020). <https://doi.org/10.1093/mnras/staa2457>, <https://arxiv.org/abs/2007.08353> [astro-ph.HE].
- [11] Lyutikov, M., Pariev, V. I. & Gabuzda, D. C. Polarization and structure of relativistic parsec-scale AGN jets. *MNRAS* **360** (3), 869–891 (2005). <https://doi.org/10.1111/j.1365-2966.2005.08954.x>, <https://arxiv.org/abs/astro-ph/0406144> [astro-ph].
- [12] Hovatta, T. *et al.* MOJAVE: Monitoring of Jets in Active Galactic Nuclei with VLBA Experiments. VIII. Faraday Rotation in Parsec-scale AGN Jets. *AJ* **144** (4), 105 (2012). <https://doi.org/10.1088/0004-6256/144/4/105>, <https://arxiv.org/abs/1205.6746> [astro-ph.CO].
- [13] Gabuzda, D. C. Inherent and Local Magnetic Field Structures in Jets from Active Galactic Nuclei. *Galaxies* **9** (3), 58 (2021). <https://doi.org/10.3390/galaxies9030058> .
- [14] Marscher, A. P. Turbulent, Extreme Multi-zone Model for Simulating Flux and Polarization Variability in Blazars. *ApJ* **780**, 87 (2014). <https://doi.org/10.1088/0004-637X/780/1/87>, <https://arxiv.org/abs/1311.7665> [astro-ph.HE].
- [15] Peirson, A. L. & Romani, R. W. The Polarization Behavior of Relativistic Synchrotron Jets. *ApJ* **864**, 140 (2018). <https://doi.org/10.3847/>

- 1538-4357/aad69d, <https://arxiv.org/abs/1807.10732> [astro-ph.HE].
- [16] Peirson, A. L. & Romani, R. W. The Polarization Behavior of Relativistic Synchrotron Self-Compton Jets. *ApJ* **885** (1), 76 (2019). <https://doi.org/10.3847/1538-4357/ab46b1>, <https://arxiv.org/abs/1909.10563> [astro-ph.HE].
- [17] Bodo, G., Tavecchio, F. & Sironi, L. Kink-driven magnetic reconnection in relativistic jets: consequences for X-ray polarimetry of BL Lacs. *MNRAS* **501** (2), 2836–2847 (2021). <https://doi.org/10.1093/mnras/staa3620>, <https://arxiv.org/abs/2006.14976> [astro-ph.HE].
- [18] Jorstad, S. G. *et al.* Polarimetric Observations of 15 Active Galactic Nuclei at High Frequencies: Jet Kinematics from Bimonthly Monitoring with the Very Long Baseline Array. *AJ* **130**, 1418–1465 (2005). <https://doi.org/10.1086/444593>, <https://arxiv.org/abs/astro-ph/0502501> .
- [19] Marin, F. A complete disclosure of the hidden type-1 AGN in NGC 1068 thanks to 52 yr of broad-band polarimetric observation. *MNRAS* **479** (3), 3142–3154 (2018). <https://doi.org/10.1093/mnras/sty1566>, <https://arxiv.org/abs/1806.04415> [astro-ph.GA].
- [20] Blinov, D. *et al.* RoboPol: AGN polarimetric monitoring data. *MNRAS* **501** (3), 3715–3726 (2021). <https://doi.org/10.1093/mnras/staa3777>, <https://arxiv.org/abs/2012.00008> [astro-ph.HE].
- [21] Weaver, Z. R. *et al.* Kinematics of Parsec-Scale Jets of Gamma-Ray Bright Blazars at 43 GHz during Ten Years of the VLBA-BU-BLAZAR Program. *ApJS* **260**, 12 (2022).
- [22] Di Gesu, L. *et al.* Testing particle acceleration models for BL LAC jets with the Imaging X-ray Polarimetry Explorer. *A&A* **662**, A83 (2022).
- [23] Angelakis, E. *et al.* RoboPol: the optical polarization of gamma-ray-loud and gamma-ray-quiet blazars. *MNRAS* **463** (3), 3365–3380 (2016). <https://doi.org/10.1093/mnras/stw2217>, <https://arxiv.org/abs/1609.00640> [astro-ph.HE].
- [24] Tavecchio, F., Landoni, M., Sironi, L. & Coppi, P. Probing dissipation mechanisms in BL Lac jets through X-ray polarimetry. *MNRAS* **480** (3), 2872–2880 (2018). <https://doi.org/10.1093/mnras/sty1491>, <https://arxiv.org/abs/1801.10060> [astro-ph.HE].
- [25] Marscher, A. P. & Jorstad, S. G. Frequency and Time Dependence of Linear Polarization in Turbulent Jets of Blazars. *Galaxies* **9** (2), 27 (2021). <https://doi.org/10.3390/galaxies9020027>, <https://arxiv.org/abs/2105.00094> [astro-ph.HE].

- [26] Comisso, L. & Sironi, L. Particle Acceleration in Relativistic Plasma Turbulence. *Phys. Rev. Lett.* **121** (25), 255101 (2018). <https://doi.org/10.1103/PhysRevLett.121.255101>, <https://arxiv.org/abs/1809.01168> [astro-ph.HE].
- [27] Marscher, A. P. *et al.* The inner jet of an active galactic nucleus as revealed by a radio-to- $\gamma$ -ray outburst. *Nat* **452**, 966–969 (2008). <https://doi.org/10.1038/nature06895>.
- [28] Sironi, L., Rowan, M. E. & Narayan, R. Reconnection-driven Particle Acceleration in Relativistic Shear Flows. *ApJL* **907** (2), L44 (2021). <https://doi.org/10.3847/2041-8213/abd9bc>, <https://arxiv.org/abs/2009.11877> [astro-ph.HE].
- [29] Tavecchio, F. Probing Magnetic Fields and Acceleration Mechanisms in Blazar Jets with X-ray Polarimetry. *Galaxies* **9** (2), 37 (2021). <https://doi.org/10.3390/galaxies9020037>, <https://arxiv.org/abs/2105.08401> [astro-ph.HE].
- [30] Webb, J. R. *et al.* The Nature of Micro-Variability in Blazars. *Galaxies* **9** (4), 114 (2021). <https://doi.org/10.3390/galaxies9040114>.
- [31] Blinov, D. *et al.* RoboPol: do optical polarization rotations occur in all blazars? *MNRAS* **462** (2), 1775–1785 (2016). <https://doi.org/10.1093/mnras/stw1732>, <https://arxiv.org/abs/1607.04292> [astro-ph.HE].

## Methods

### X-ray polarization observations

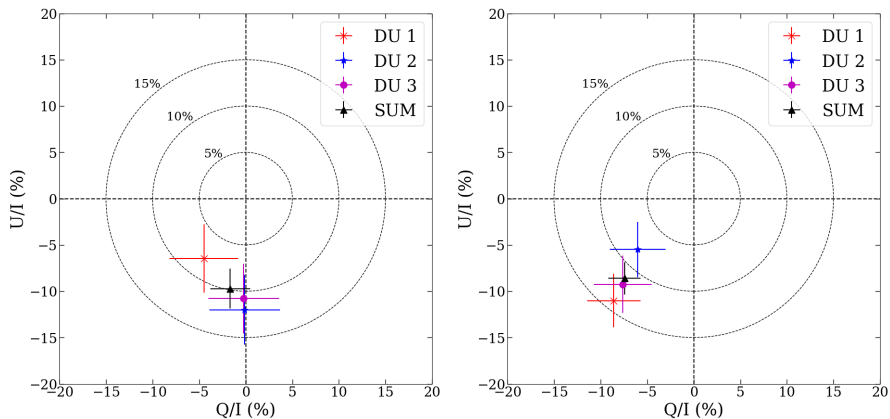
*IXPE* is a joint mission of the U.S. National Aeronautics and Space Administration and the Italian Space Agency (Agenzia Spaziale Italiana). A description of the spacecraft and of the payload is given by [2]; the detector units are described in [32]. Mrk 501 was observed with *IXPE* over an effective exposure time of 100 ksec from 8 to 10 March 2022 (MJD 59646–59648) and again from 26–28 March 2022 (MJD 59664–59666) for 86 ksec. The exposure times were selected based on [33], which determined that a 100 ksec exposure would be sufficient to measure polarization in Mrk 501 in a blind survey. At the  $\sim 30''$  angular resolution of *IXPE*, Mrk 501 is essentially a point source.

The *IXPE* raw (level-1) data were first reduced and corrected for instrumental polarization artifacts as well as boom and spacecraft motion to create level-2 event files (L2). The L2 data were then corrected for the energy scaling of the detector and bad aspect time intervals following standard procedures within the latest version of the *ixpeobssim* pipeline [34, 35]. The *IXPE* L2 files contain the polarization information in the form of photon-by-photon Stokes parameters. All the quoted results refer

to the average of the three identical IXPE detector units (DU). We selected source photons using *xpselect* and a circular region with a radius of 60'' centered on the source. The polarization degree and angle was determined in the 2-8 keV energy range using three different analysis techniques performed by five independent groups to ensure an unbiased estimation. Those techniques were a model-independent analysis, spectropolarimetric fit in XSPEC, and a maximum likelihood spectropolarimetric (MLS) fit implemented within the MULTINEST algorithm. Although the effect of the photoelectric absorption is negligible over the 2-8 keV energy range of *IXPE*, the spectropolarimetric fits included photoelectric absorption based on the measured Galactic neutral hydrogen column density toward Mrk 501 of  $N_H = 1.69 \times 10^{20} \text{ cm}^{-2}$  [37]. The model-independent analysis applies the [38] formalism to a user-defined subset of photons and determines the total Stokes parameters. We have performed both a weighted and unweighted analysis. In the model-independent analysis we do not perform background subtraction. We found that the sky background counts for a 60'' region are only 3% of the total counts. We have verified that for a bright blazar such as Mrk 501, the background has a negligible effect on the polarization analysis. For the spectropolarimetric fits, we simultaneously fit 3 × I, Q, U spectra (one set from each *IXPE* – DU). In XSPEC, following the approach of [36], we used an absorbed single power-law component with constant  $\Pi$  and  $\psi$  (CONSTPOL model). For the MLS fit, we used a single power-law spectral component with constant intrinsic Q and U values. Given the exposure time and flux of Mrk 501 at the time of the *IXPE* observations, the minimum degree of detectable polarization at a 99% confidence level (MDP99) we were able to achieve is 6.6% for the 8-10 March, and 5.2% for the 26-28 March observation. The source was brighter in X-rays during the 26-28 March observation (see below), hence the lower MDP99. The derived  $\Pi$  and  $\psi$  for the different methods are summarized in Table 2 for both observations. In both cases, all the measurements through the different analyses are consistent within the uncertainties with the median linear X-ray  $\Pi$  and  $\psi$  of  $\Pi_X = 10 \pm 2\%$ ,  $\psi_X = 134^\circ \pm 5^\circ$  and  $\Pi_X = 11 \pm 2\%$ ,  $\psi_X = 115^\circ \pm 4^\circ$  respectively. Figure 2 shows the Stokes Q/I and Stokes U/I of our observation along with the MDP99. Depending on the emission model, variability time scales are expected to range from sub-day to a few days [e.g., 22]. A 16-day interval between observations allows us to look for variability on a few days time scale which, however, we do not find. We have also searched for variability within the individual *IXPE* observations. This was done by splitting the *IXPE* exposures in two and three equal size time-bins. We again do not find evidence for variability within the uncertainties.

**Table 2** Median polarization degree and angle measurements from the *IXPE* data analysis performed by independent groups using three analysis techniques.

Date	Method	$\Pi$ (%)	$\psi$ (degrees)
8-10 March	Model-independent	$10.5 \pm 2.1$	$130 \pm 6$
	XSPEC	$10.5 \pm 1.8$	$135 \pm 5$
	MLS	$10.6^{+1.7}_{-1.6}$	$135 \pm 5$
26-28 March	Model-independent	$11.5 \pm 1.6$	$115 \pm 4$
	XSPEC	$10.7 \pm 1.5$	$115 \pm 4$
	MLS	$10.6 \pm 1.5$	$115 \pm 4$

**Fig. 2** Stokes Q/I and Stokes U/I parameters of our *IXPE* observations during 8-10 March 2022 (left) and 26-28 March 2022 (right). The measurements are shown for the three detectors (DU1 [red x], DU2 [blue star], DU3 [magenta circle]) separately and combined (black triangle). The red shaded regions denote the value of MDP99.

## Multiwavelength Observations

Here we report on a subset of our contemporaneous multiwavelength campaign from radio to TeV  $\gamma$ -rays which is summarized in Tables 3, 4 and Fig. 3. The complete multiwavelength dataset will be presented in a forthcoming paper.

### Millimeter-radio observations

Polarimetric millimeter radio measurements at 3.5 mm (86.24 GHz) and 1.3 mm (230 GHz) were obtained with the 30 m Telescope of the Institut de Radioastronomie Millimétrique (IRAM), located at the Pico Veleta Observatory (Sierra Nevada, Granada, Spain), on 9-10 March 2022 (MJD 59647-59649), within the Polarimetric Monitoring of AGN at Millimeter Wavelengths (POLAMI) program<sup>1</sup> [39–41]. Weather related reasons prevented us from obtaining radio observations during the second *IXPE* exposure. Under the POLAMI observing setup, the four Stokes parameters (I, Q, U, and V) are recorded simultaneously using the XPOL

<sup>1</sup><http://polami.iaa.es/>

procedure [42]. The data reduction, calibration, and managing and flagging procedures used in POLAMI are thoroughly described in [39]. The source was relatively stable in flux during the observations at both 1.3 and 3.5 mm with total flux densities of  $0.71\pm 0.04$  Jy and  $0.73\pm 0.04$  Jy at 3.5 mm, and  $0.41\pm 0.02$  Jy and  $0.39\pm 0.02$  Jy at 1.3 mm, on 9 and 10 of March respectively. Also, the polarized flux at 3.5 mm remained stable both in linear polarization degree and angle between the two dates. No polarization above 3.46% (95% confidence upper limit) was detected at 1.3 mm.

### ***Optical and infrared observations***

Optical polarization observations were performed using several telescopes across the world: the Nordic Optical Telescope (NOT) on the night of 8-9 March (MJD 59647); the Tohoku 60 cm (T60) telescope at the Haleakala Observatory on 10 March (MJD 59649) and on 28 March (MJD 59667); the 2.2m Calar Alto Observatory and 1.5m Sierra Nevada Observatory telescopes on 8-10 March; the AZT-8 telescope of the Crimean Astrophysical Observatory and the St. Petersburg State University LX-200 telescope during 8-10 March and 25-28 March.

The NOT observations used the Alhambra Faint Object Spectrograph and Camera (ALFOSC) in four bands (BVRI) in the standard polarimetric mode. The data were then analyzed with the semi-automatic pipeline developed at the Tuorla Observatory using standard photometric procedures [43, 44]. Both highly-polarized and unpolarized standard stars were observed during the same night for calibration purposes. The T60 polarimetric measurements were performed using the Dipol-2 polarimeter [45]. Dipol-2 is a remotely operated double-image CCD polarimeter, which is capable of recording polarized images in three (BVR) filters simultaneously [46–49]. We obtained 24 individual measurements of the Stokes Q/I and U/I parameters simultaneously in three filters (BVR). Twenty unpolarized and two highly-polarized (HD204827 and HD25443) nearby standard stars were observed for calibration and determination of the polarization angle zero point. The individual measurements were used to compute nightly average values using the “ $2 \times$  sigma-weighting algorithm”. The algorithm iteratively filters out outliers, assigning smaller weights to these measurements. The errors on the Stokes Q/I and U/I parameters were computed as standard errors of the weighted means. These errors were then used to estimate uncertainties on the polarization degree and angle [49, 50]. The Calar Alto Observatory observations were performed in the Johnson Cousins  $R_c$  optical band by the Calar Alto Faint Object Spectrograph (CAFOS) in imaging polarimetric mode on the 2.2m Telescope. The data were reduced following standard analysis procedures using both unpolarized and polarized standard stars for calibration purposes. Similarly, Mrk 501 was observed by the 1.5 m telescope at Sierra Nevada Observatory using polarized  $R_c$  filters during the

three nights. The 70cm AZT-8 telescope and the 40cm LX-200 telescope observations were carried out in the Cousins R band. Both telescopes are equipped with nearly identical imaging photometers-polarimeters based on a ST-7 camera. Two Savart plates rotated by 45 deg relative to each other are swapped to measure the relative Stokes q and u parameters from the two split images of each source in the field. The polarization parameters for each observation are produced by the sum of  $15 \times 30$ s consecutive exposures. The data are then corrected for bias, flat field, background level, and calibrated for instrumental and interstellar polarization using the (assumed) unpolarized comparison stars 1, 4, and 6 from [51]. The same stars were used to perform differential photometry. During both *IXPE* observations, all the optical polarization observations are within uncertainties, which suggests no significant variability.

Observations were also obtained with the WIRC+Pol instrument [52] on the 200-inch Palomar Hale telescope in J band. WIRC+Pol uses a polarizing grating to disperse the light into four beams that sense the four different components of linear polarization ( $0^\circ$ ,  $45^\circ$ ,  $90^\circ$ ,  $135^\circ$ ), and a half-wave plate for beam swapping to improve polarimetric sensitivity [53, 54]. Data reduction made use of the WIRC+Pol Data Reduction Pipeline software<sup>2</sup> [52]. The pipeline software averages the measurements over the course of the half-wave plate rotation cycles to account for subtle differences in light paths through the instrument, and reports the degree and angle of polarization in each band. The results were verified with the use of both polarized and unpolarized standard stars. For additional details on the data reduction, see [55].

The starlight from the host galaxy (assumed to be unpolarized) of Mrk 501 contributes a significant fraction of the optical flux. For this reason, the observed  $\Pi_{\text{O}}$  needs to be corrected for the depolarization effect of the host-galaxy. To achieve this, we need to estimate the contribution of the host galaxy ( $I_{\text{host}}$ , in mJy) within the aperture used for the analysis of individual observations. Due to the instrumental setup, observations from the T60 and Palomar-Hale telescopes are not used for this calculation. For this reason, the measurements from T60 (R-band) and Hale (J-band) should be treated as lower limits to the intrinsic polarization degree. The light profile of Mrk 501's host galaxy has been fully characterized in the R-band in [56]. This allows us to estimate  $I_{\text{host}}$  for each observation separately. We then subtract  $I_{\text{host}}$  from the total intensity  $I$  and estimate the intrinsic polarization degree following [43] as  $\Pi_{\text{intr}} = \Pi_{\text{obs}} \times I / (I - I_{\text{host}})$ . We calculate  $\Pi_{\text{intr}}$  in the R-band for each observation and then estimate a median. We find the median intrinsic polarization degree and its uncertainty to be  $\Pi_{\text{intr}} = 4 \pm 1\%$  for the 8-10 March observation and  $\Pi_{\text{intr}} = 5 \pm 1\%$  for the 26-28 March observation. Figure 3 shows the multiwavelength polarization degree from radio to X-rays.

---

<sup>2</sup>[https://github.com/WIRC-Pol/wirc\\_drp](https://github.com/WIRC-Pol/wirc_drp)

**X-ray observations**

During the *IXPE* observations we independently measured the X-ray total flux and spectrum with the X-Ray Telescope (XRT, [57]) on the orbiting Neil Gehrels *Swift* Observatory (*Swift*) in Window Timing mode (WT, 4×1 ksec exposures – 2×1 ksec for each *IXPE* observation) and with the Nuclear Spectroscopic Telescope Array (*NuSTAR*, 20 ksec exposure, [58]) during the 8-10 March observation. We extracted the X-ray spectrum from each telescope following standard analysis procedures and the latest calibration data files. For the source regions we used a circular radius of 47'' and 49'' for *Swift* and *NuSTAR*, respectively. To estimate the background for the *NuSTAR* spectra we used a 147'' circular region outside of the region containing significant photon counts from Mrk 501. The background for *Swift* was extracted using the same size circular region from an available blank sky WT observation from the *Swift* archive. For the 8-10 March observation, we fit the combined *Swift* and *NuSTAR* data in *XSPEC* with an absorbed log-parabola model  $N(E) = (E/E_p)^{-\alpha-\beta \log(E/E_p)}$ , in the 0.3-79 keV energy range.  $N_H$  was set to the Galactic value, and the pivot energy was set to  $E_p = 5$  keV. This model provides a reasonably good fit to the data ( $\chi^2/\text{dof} = 862/850$ ) with best-fit parameters  $\alpha = 2.27 \pm 0.01$  and  $\beta = 0.28 \pm 0.01$ . We also tested a single power-law model, however, there is clear curvature in the spectrum and the fit is statistically worse ( $\chi^2/\text{dof} = 2005/851$ ). We measure the flux of the source in the 2-8 keV range to be  $10 \pm 0.5 \times 10^{-11}$  erg/s/cm<sup>2</sup>. We do not find evidence for variability during the *IXPE* observations. For the 26-28 March observation we follow the same procedure using only the available *Swift* data. The source was in a higher flux state with  $\alpha = 2.05 \pm 0.02$  and  $\beta = 0.26 \pm 0.04$  and flux in the 0.3-10 keV range of  $21 \pm 0.6 \times 10^{-11}$  erg/s/cm<sup>2</sup>. The *Swift* observations show a change from 12 to 14 counts/sec (17% increase) from the beginning until the end of the *IXPE* observation. The results from our multiwavelength campaign are summarized in Tables 3 and 4.

**Activity state of Mrk 501**

Mrk 501 is a BL Lac type object at a redshift of  $z = 0.033$ , corresponding to a luminosity distance of 141.3 Mpc<sup>3</sup>, and a synchrotron peak frequency  $\nu_{\text{syn}} \sim 2.8 \times 10^{15}$  Hz [60]. It is among the brightest sources in the sky at very high  $\gamma$ -ray energies ( $\geq 0.1$  Tev), and is well-studied across the electromagnetic spectrum [e.g., 61–65]. We use archival data from *Swift*<sup>4</sup>, Steward observatory [66]<sup>5</sup>, the RoboPol program<sup>6</sup> [20], and the Boston University (BU) blazar monitoring program<sup>7</sup> to build the long-term light

<sup>3</sup>Assuming a flat  $\Lambda$ CDM cosmological model with  $\Omega_m = 0.27$  and  $H_0 = 71$  km/s/Mpc [59].

<sup>4</sup><https://www.swift.psu.edu/monitoring/>

<sup>5</sup><http://james.as.arizona.edu/~psmith/Fermi/>

<sup>6</sup><http://robopol.physics.uoc.gr/>

<sup>7</sup><https://www.bu.edu/blazars/index.html>

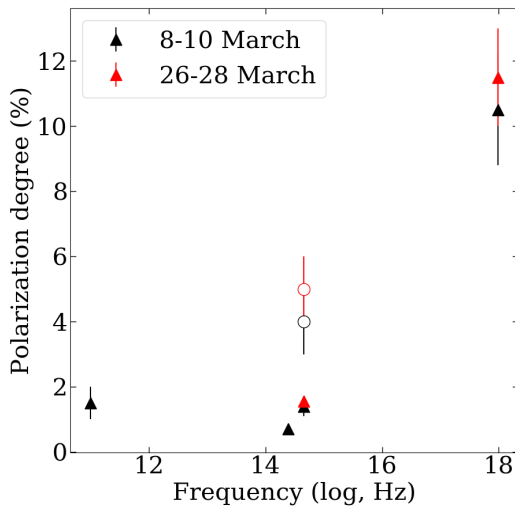


**Fig. 3** Multiwavelength polarization degree of Mrk 501 from radio to X-rays. Black symbols are for the 8-10 March observation, and red for the 26-28 March observation. The open symbols show the host-galaxy corrected – intrinsic optical polarization degree.

**Table 3** Multiwavelength and polarization observations for the 2022 March 8-10 observation.

Telescope	Flux density (Jy)	Radio $\Pi$ (%)	Radio $\psi$ (degrees)
IRAM 30m (3.5mm)	$0.72 \pm 0.04$	$1.5 \pm 0.5$	$152 \pm 10$
IRAM 30m (1.3mm)	$0.4 \pm 0.02$	–	–
Telescope	Magnitude	Optical $\Pi$ (%)	Optical $\psi$ (degrees)
Calar Alto 2.2m	$13.15 \pm 0.01$	$1.6 \pm 0.5$	$118 \pm 10$
LX-200	$13.16 \pm 0.01$	$1.3 \pm 0.3$	$129 \pm 6$
NOT	$13.83 \pm 0.01$	$2.1 \pm 0.3$	$116 \pm 5$
Palomar-Hale	–	$0.7 \pm 0.1$	$111 \pm 6$
Sierra Nevada Observatory 1.5m	$13.18 \pm 0.01$	$1.8 \pm 0.8$	$123 \pm 12$
T60	$13.87 \pm 0.01$	$1.7 \pm 0.08$	$116 \pm 2$
Telescope	X-ray flux ( $\times 10^{-11}$ erg/s/cm <sup>2</sup> )	X-ray $\Pi$ (%)	X-ray $\psi$ (degrees)
<i>IXPE</i>	$8.8 \pm 0.1$	$10 \pm 2$	$134 \pm 5$
<i>Swift + NuSTAR</i>	$10.0 \pm 0.5$	–	–

The millimeter-radio flux density is in Janskys. For the millimeter-radio and optical observations we report the median estimate of the observations during the *IXPE* observation. The listed uncertainty is either the standard deviation of the measurements or the median uncertainty, whichever is larger. For the NOT and T60 analysis we used a circular  $1.5''$  radius aperture. For the data analysis of remaining optical telescopes we used a  $7.5''$  aperture. The Palomar observations are in the J-band.  $\psi$  is given in degrees. The X-ray fluxes are estimated in the 2-8 keV range, and given in units of  $10^{-11}$  erg/s/cm<sup>2</sup>.

**Table 4** Multiwavelength and polarization observations for the 2022 March 26-28 observation.

Telescope	Magnitude	Optical $\Pi$ (%)	Optical $\psi$ (degrees)
AZT-8	13.15±0.01	1.5±0.2	117±3
T60	13.52±0.01	1.8±0.1	115±2
Telescope	X-ray flux ( $\times 10^{-11}$ erg/s/cm <sup>2</sup> )	X-ray $\Pi$ (%)	X-ray $\psi$ (degrees)
<i>IXPE</i>	18.0±0.4	11±2	115±4
<i>Swift</i>	21.0±0.6	-	-

Same as in Table 3.

curves of Mrk 501 in optical brightness (R-band magnitude), optical polarization degree, polarization angle, and X-ray flux (Fig. 4). The optical observations cover a range from October 2008 up to June 2021. At R band, the source varied between 13.53<sup>m</sup> and 13.24<sup>m</sup>, with a median of 13.4<sup>m</sup>. The median observed  $\Pi_O$  (not corrected for the host-galaxy contribution) was 2.1% with a minimum of 0.07% and a maximum of 5.9%. The  $\psi_O$  typically fluctuates about the jet axis ( $120^\circ \pm 12^\circ$ ) with a median of 136°, and a minimum and maximum of 65° and 171° respectively. The X-ray observations cover a range from April 2005 until June 2020. The median X-ray flux in the 0.3-10 keV was  $15 \times 10^{-11}$  erg/s/cm<sup>2</sup>, with a minimum and maximum at around  $3.7 \times 10^{-11}$  erg/s/cm<sup>2</sup> and  $76 \times 10^{-11}$  erg/s/cm<sup>2</sup>, respectively. At the time of the *IXPE* observations our multiwavelength campaign finds the flux and polarization of the source within one standard deviation from the median of the respective light curve. For the first *IXPE* observation the X-ray flux of the source seems to correspond to an average state, while in the second observation we find the source in an elevated-flux state.

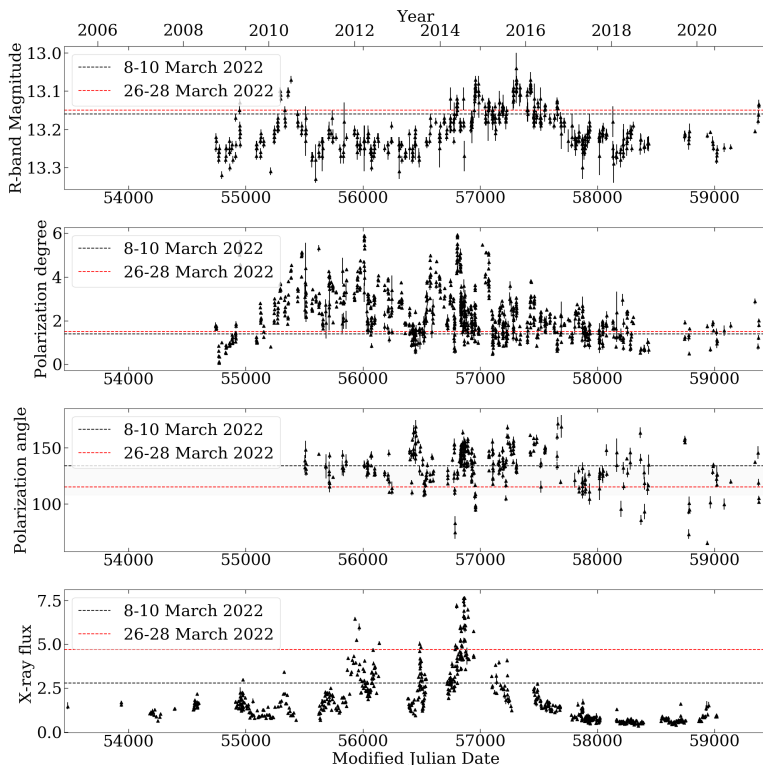


**Fig. 4** Archival optical brightness (R-band, upper panel), observed optical  $\psi$  (third-from-top panel), and X-ray flux (lower panel) light curves for Mrk 501. The black and red dashed line indicate the level of the source during the 8-10 March and 26-28 March *IXPE* observations respectively. The grey shaded area in the  $\psi$  shows the direction of the jet axis.

## References

- [32] P. Soffitta, L. Baldini, R. Bellazzini, E. Costa, L. Latronico, F. Muleri, E.D. Monte, S. Fabiani, M. Minuti, M. Pinchera, C. Sgro', G. Spandre, A. Trois, F. Amici, H. Andersson, P. Attina', M. Bachetti, M. Barbanera, F. Borotto, A. Brez, D. Brienza, C. Caporale, C. Cardelli, R. Carpentiero, S. Castellano, M. Castronuovo, L. Cavalli, E. Cavazzuti, M. Ceccanti, M. Centrone, S. Ciprini, S. Citraro, F. D'Amico, E. D'Alba, S.D. Cosimo, N.D. Lalla, A.D. Marco, G.D. Persio, I. Donnarumma, Y. Evangelista, R. Ferrazzoli, A. Hayato, T. Kitaguchi, F.L. Monaca, C. Lefevre, P. Lofredo, P. Lorenzi, L. Lucchesi, C. Magazzu, S. Maldera, A. Manfreda, E. Mangraviti, M. Marengo, G. Matt, P. Mereu, A. Morbidini, F. Mosti, T. Nakano, H. Nasimi, B. Negri, S. Nenonen, A. Nuti, L. Orsini, M. Perri, M. Pesce-Rollins, R. Piazzolla, M. Pilia, A. Profeti, S. Puccetti, J. Rankin, A. Ratheesh, A. Rubini, F. Santoli, P. Sarra, E. Scalise, A. Sciortino,

- T. Tamagawa, M. Tardiola, A. Tobia, M. Vimercati, F. Xie, The instrument of the imaging x-ray polarimetry explorer. *The Astronomical Journal* **162**(5), 208 (2021). <https://doi.org/10.3847/1538-3881/ac19b0>. URL <https://doi.org/10.3847/1538-3881/ac19b0>
- [33] Liodakis, I., Peirson, A. L. & Romani, R. W. Prospects for Detecting X-ray Polarization in Blazar Jets. *The Astrophysical Journal* **880**, 7 (2019). <https://doi.org/10.3847/1538-4357/ab2719> . <https://arxiv.org/abs/1906.01647> [astro-ph.IM].
- [34] Pesce-Rollins, M., Lalla, N. D., Omodei, N. & Baldini, L. An observation-simulation and analysis framework for the Imaging X-ray Polarimetry Explorer (IXPE). *Nuclear Instruments and Methods in Physics Research A* **936**, 224–226 (2019). <https://doi.org/10.1016/j.nima.2018.10.041> .
- [35] Baldini, L. *et al.* ixpeobssim: a Simulation and Analysis Framework for the Imaging X-ray Polarimetry Explorer. *arXiv e-prints* arXiv:2203.06384 (2022). <https://arxiv.org/abs/2203.06384> [astro-ph.IM].
- [36] Strohmayer, T. E. X-Ray Spectro-polarimetry with Photoelectric Polarimeters. *ApJ* **838** (1), 72 (2017).
- [37] Kalberla, P. M. W. *et al.* The Leiden/Argentine/Bonn (LAB) Survey of Galactic HI. Final data release of the combined LDS and IAR surveys with improved stray-radiation corrections. *A&A* **440** (2), 775–782 (2005). <https://doi.org/10.1051/0004-6361:20041864>, <https://arxiv.org/abs/astro-ph/0504140> [astro-ph].
- [38] Kislat, F., Clark, B., Beilicke, M. & Krawczynski, H. Analyzing the data from X-ray polarimeters with Stokes parameters. *Astroparticle Physics* **68**, 45–51 (2015). <https://doi.org/10.1016/j.astropartphys.2015.02.007>, <https://arxiv.org/abs/1409.6214> [astro-ph.IM].
- [39] Agudo, I. *et al.* POLAMI: Polarimetric Monitoring of AGN at Millimetre Wavelengths - I. The programme, calibration and calibrator data products. *MNRAS* **474** (2), 1427–1435 (2018). <https://doi.org/10.1093/mnras/stx2435>, <https://arxiv.org/abs/1709.08742> [astro-ph.GA].
- [40] Agudo, I. *et al.* POLAMI: Polarimetric Monitoring of Active Galactic Nuclei at Millimetre Wavelengths - III. Characterization of total flux density and polarization variability of relativistic jets. *MNRAS* **473** (2), 1850–1867 (2018). <https://doi.org/10.1093/mnras/stx2437>, <https://arxiv.org/abs/1709.08744> [astro-ph.GA].
- [41] Thum, C. *et al.* POLAMI: Polarimetric Monitoring of Active Galactic Nuclei at Millimetre Wavelengths - II. Widespread circular polarization. *MNRAS* **473** (2), 2506–2520 (2018). <https://doi.org/10.1093/mnras/>

- stx2436, <https://arxiv.org/abs/1709.08743> [astro-ph.GA].
- [42] Thum, C., Wiesemeyer, H., Paubert, G., Navarro, S. & Morris, D. XPOL—the Correlation Polarimeter at the IRAM 30-m Telescope. *PASP* **120** (869), 777 (2008). <https://doi.org/10.1086/590190>, <https://arxiv.org/abs/0806.1666> [astro-ph].
- [43] Hovatta, T. *et al.* Optical polarization of high-energy BL Lacertae objects. *A&A* **596**, A78 (2016). <https://doi.org/10.1051/0004-6361/201628974>, <https://arxiv.org/abs/1608.08440> [astro-ph.HE].
- [44] Nilsson, K. *et al.* Long-term optical monitoring of TeV emitting blazars. I. Data analysis. *A&A* **620**, A185 (2018). <https://doi.org/10.1051/0004-6361/201833621>, <https://arxiv.org/abs/1810.01751> [astro-ph.HE].
- [45] Piirola, V., Berdyugin, A. & Berdyugina, S. Ramsay, S. K., McLean, I. S. & Takami, H. (eds) *DIPOL-2: a double image high precision polarimeter*. (eds Ramsay, S. K., McLean, I. S. & Takami, H.) *Ground-based and Airborne Instrumentation for Astronomy V*, Vol. 9147 of *Society of Photo-Optical Instrumentation Engineers (SPIE) Conference Series*, 91478I (2014).
- [46] Piirola, V. A double image chopping polarimeter. *A&A* **27**, 383–388 (1973) .
- [47] Berdyugin, A. V., Berdyugina, S. V. & Piirola, V. Evans, C. J., Simard, L. & Takami, H. (eds) *High-precision and high-accuracy polarimetry of exoplanets*. (eds Evans, C. J., Simard, L. & Takami, H.) *Ground-based and Airborne Instrumentation for Astronomy VII*, Vol. 10702 of *Society of Photo-Optical Instrumentation Engineers (SPIE) Conference Series*, 107024Z (2018).
- [48] Berdyugin, A., Piirola, V. & Poutanen, J. Mignani, R., Shearer, A., Słowikowska, A. & Zane, S. (eds) *Optical Polarimetry: Methods, Instruments and Calibration Techniques*. (eds Mignani, R., Shearer, A., Słowikowska, A. & Zane, S.) *Astronomical Polarisation from the Infrared to Gamma Rays*, Vol. 460 of *Astrophysics and Space Science Library*, 33 (2019). [1908.10431](https://doi.org/10.1007/978-94-007-5100-0_33).
- [49] Piirola, V., Kosenkov, I. A., Berdyugin, A. V., Berdyugina, S. V. & Poutanen, J. Double Image Polarimeter—Ultra Fast: Simultaneous Three-color (BV R) Polarimeter with Electron-multiplying Charge-coupled Devices. *AJ* **161** (1), 20 (2021). <https://doi.org/10.3847/1538-3881/abc74f> .
- [50] Kosenkov, I. A. *et al.* High-precision optical polarimetry of the accreting black hole V404 Cyg during the 2015 June outburst. *MNRAS* **468** (4), 4362–4373 (2017). <https://doi.org/10.1093/mnras/stx779>, <https://arxiv.org/abs/1709.08743>.

[org/abs/1702.02008](https://doi.org/abs/1702.02008) [astro-ph.HE].

- [51] Villata, M., Raiteri, C. M., Lanteri, L., Sobrito, G. & Cavallone, M. BVR photometry of comparison stars in selected blazar fields. I. Photometric sequences for 10 BL Lacertae objects. *Ap&SS* **130**, 305–310 (1998). <https://doi.org/10.1051/aas:1998415> .
- [52] Tinyanont, S. *et al.* WIRC+Pol: A Low-resolution Near-infrared Spectropolarimeter. *PASP* **131** (996), 025001 (2019). <https://doi.org/10.1088/1538-3873/aaef0f>, <https://arxiv.org/abs/1811.03138> [astro-ph.IM].
- [53] Tinyanont, S. *et al.* *Achieving a spectropolarimetric precision better than 0.1% in the near-infrared with WIRC+Pol*, Vol. 11132 of *Society of Photo-Optical Instrumentation Engineers (SPIE) Conference Series*, 1113209 (2019). [1908.10409](https://doi.org/10.1117/12.2562762).
- [54] Millar-Blanchaer, M. A. *et al.* Evans, C. J., Bryant, J. J. & Motohara, K. (eds) *WIRC-POL: 0.1polarimetric precision on-sky with the installation of a HWP modulator*. (eds Evans, C. J., Bryant, J. J. & Motohara, K.) *Ground-based and Airborne Instrumentation for Astronomy VIII*, Vol. 11447, 1315 – 1332. International Society for Optics and Photonics (SPIE, 2021). URL <https://doi.org/10.1117/12.2562762>.
- [55] Masiero, J. R., Tinyanont, S. & Millar-Blanchaer, M. A. Asteroid Polarimetric-Phase Behavior in the Near-Infrared: S- and C-Complex Objects. *arXiv e-prints* arXiv:2203.15790 (2022). <https://arxiv.org/abs/2203.15790> [astro-ph.EP].
- [56] Nilsson, K. *et al.* Host galaxy subtraction of TeV candidate BL Lacertae objects. *A&A* **475** (1), 199–207 (2007). <https://doi.org/10.1051/0004-6361:20077624>, <https://arxiv.org/abs/0709.2533> [astro-ph].
- [57] Burrows, D. N. *et al.* The Swift X-Ray Telescope. *Space Sci. Rev.* **120** (3–4), 165–195 (2005). <https://doi.org/10.1007/s11214-005-5097-2>, <https://arxiv.org/abs/astro-ph/0508071> [astro-ph].
- [58] Harrison, F. A. *et al.* The Nuclear Spectroscopic Telescope Array (NuSTAR) High-energy X-Ray Mission. *ApJ* **770** (2), 103 (2013). <https://doi.org/10.1088/0004-637X/770/2/103>, <https://arxiv.org/abs/1301.7307> [astro-ph.IM].
- [59] Komatsu, E. *et al.* Five-Year Wilkinson Microwave Anisotropy Probe Observations: Cosmological Interpretation. *ApJS* **180**, 330–376 (2009). <https://doi.org/10.1088/0067-0049/180/2/330>, <https://arxiv.org/abs/0803.0547> .

- [60] Ajello, M. *et al.* The Fourth Catalog of Active Galactic Nuclei Detected by the Fermi Large Area Telescope. *ApJ* **892** (2), 105 (2020). <https://doi.org/10.3847/1538-4357/ab791e>, <https://arxiv.org/abs/1905.10771> [astro-ph.HE].
- [61] Quinn, J. *et al.* Detection of Gamma Rays with E  $\geq$  300 GeV from Markarian 501. *ApJL* **456**, L83 (1996). <https://doi.org/10.1086/309878>.
- [62] Abdo, A. A. *et al.* Insights into the High-energy  $\gamma$ -ray Emission of Markarian 501 from Extensive Multifrequency Observations in the Fermi Era. *ApJ* **727** (2), 129 (2011). <https://doi.org/10.1088/0004-637X/727/2/129>, <https://arxiv.org/abs/1011.5260> [astro-ph.HE].
- [63] Aleksić, J. *et al.* Multiwavelength observations of Mrk 501 in 2008. *A&A* **573**, A50 (2015). <https://doi.org/10.1051/0004-6361/201322906>, <https://arxiv.org/abs/1410.6391> [astro-ph.HE].
- [64] Ahnen, M. L. *et al.* Multiband variability studies and novel broadband SED modeling of Mrk 501 in 2009. *A&A* **603**, A31 (2017). <https://doi.org/10.1051/0004-6361/201629540>, <https://arxiv.org/abs/1612.09472> [astro-ph.HE].
- [65] Arbet-Engels, A. *et al.* Long-term multi-band photometric monitoring of Mrk 501. *arXiv e-prints* arXiv:2109.03205 (2021). <https://arxiv.org/abs/2109.03205> [astro-ph.HE].
- [66] Smith, P. S. *et al.* Coordinated Fermi/Optical Monitoring of Blazars and the Great 2009 September Gamma-ray Flare of 3C 454.3. *arXiv e-prints* arXiv:0912.3621 (2009). <https://arxiv.org/abs/0912.3621> [astro-ph.HE].